*materials*

MDPI

*Article*

# Genetic Algorithm-Assisted Design of Sandwiched One-Dimensional Photonic Crystals for Efficient Fluorescence Enhancement of 3.18-μm-Thick Layer of the Fluorescent Solution

**Jiantong Song [1,2], Guang Feng [1,2], Xiao Liu [1,2], Haoqiang Hou [1,2] and Zhihui Chen [1,2,*]**

[1] Key Lab of Advanced Transducer and Intelligent Control System, Ministry of Education and Shanxi Province, Taiyuan University of Technology, Taiyuan 030024, China
[2] College of Physics and Optoelectronics, Taiyuan University of Technology, Taiyuan 030024, China
* Correspondence: huixu@126.com

**Abstract:** One-dimensional photonic crystal structures have been widely used to enhance fluorescence. However, its fluorescence enhancement is low-fold because of a weak excitation field region. In this paper, we used a genetic algorithm to assist in the design of two photonic crystals based on $Al_2O_3$ and $TiO_2$ materials. One of them has a defect consisting of $SiO_2$. The Fabry-Perot cavity (FP cavity) formed by the sandwiched photonic crystal achieves up to 14-fold enhancement of the excitation electric field. We modulate the electric field radiation distribution of the fluorescent material by using photonic forbidden bands. For a 3.18 μm thick layer of the fluorescent solution, the structure achieves up to 60-fold fluorescence enhancement. We also discussed that the reason for the different enhancement abilities in different places is the phase change caused by the optical path difference. This design is expected to have applications in display, imaging, etc.

**Keywords:** one-dimensional photonic crystal; fluorescence enhancement; genetic algorithm

check for updates

**Citation:** Song, J.; Feng, G.; Liu, X.; Hou, H.; Chen, Z. Genetic Algorithm-Assisted Design of Sandwiched One-Dimensional Photonic Crystals for Efficient Fluorescence Enhancement of 3.18-μm-Thick Layer of the Fluorescent Solution. *Materials* **2022**, *15*, 7803. https://doi.org/10.3390/ma15217803

Academic Editor: Toma Stoica

Received: 16 September 2022
Accepted: 14 October 2022
Published: 4 November 2022

**Publisher's Note:** MDPI stays neutral with regard to jurisdictional claims in published maps and institutional affiliations.

**Copyright:** © 2022 by the authors. Licensee MDPI, Basel, Switzerland. This article is an open access article distributed under the terms and conditions of the Creative Commons Attribution (CC BY) license (https://creativecommons.org/licenses/by/4.0/).

## 1. Introduction

Fluorescence-enhanced structures are widely designed for environmental monitoring, biochemical, medical, and display applications [1–6]. Many studies have been conducted to investigate structures for localized fluorescence enhancement, and these studies often use surface plasmas [7,8], resonant cavities [9–12], and photonic crystals [13,14] to achieve fluorescence enhancement. For example, Boxiang Song et al. [15] designed a structure with a gold sphere as the tip with the excitation electric field localized between the gold spheres; Jungeun Song et al. [16] designed a triangular hole and circular hole array structure with the excitation electric field concentrated in the holes; Nikhil Ganesh et al. [17] designed a perforated photonic crystal with the electric field similarly concentrated in the holes. Songtao Hu et al. [18] coated quantum dots among the gaps of opal structures, which is also the region with the strongest excitation field. However, local area fluorescence enhancement tends to focus on certain hot spots. For large-area fluorescence enhancement, some hot spots will lead to overexcitation of fluorescent material in some regions and low utilization of fluorescent material in other non-hot areas, leading to low overall fluorescence utilization and decreased device lifetime.

Some studies have explored considerable area fluorescence enhancement, e.g., Markus Nyman et al. [19] used surface plasmon as an enhanced excitation field. Weina Zhang et al. [20] also used surface plasmon in combination with microlenses to achieve 260-fold enhancement, but the electric field strength of surface plasmon decays substantially with propagation distance. This means that the layer of fluorescent material cannot be increased in thickness. Hongyun Xuan et al. [21] assembled a one-dimensional photonic crystal with ZnO spheres and coated the quantum dots on the sphere surface, and such a structure

obtained a specific excitation electric field enhancement on the sphere surface. Patrick et al. [22] designed a two-dimensional photonic crystal structure to achieve full-plane enhancement, but its enhancement multiplicity varied considerably at different horizontal positions. Ehsan Eftekhar et al. [23] used an opal structure to construct a resonant cavity to achieve fluorescence enhancement of Rhodamine B, but the enhancement multiplicity was not high. Besides, one-dimensional photonic crystals enable large-area fluorescence enhancement. The work of combining photonic crystal and fluorescence enhancement always regards the photonics crystal as a non-loss structure of reflector [24–27]. Without adding other structures, the one-dimensional photonic crystals own a low fold. As a result, a fluorescence enhancement structure with a large area and high magnification need to be designed. Some works add the fluorescence material as a part of the photonic crystal. But these layers' depths are usually lower than one-quarter of the wavelength [28–30]. In summary, there are no structures to achieve efficient enhancement in a large area and a high-thickness layer of fluorescent material.

Therefore, we propose to realize fluorescence enhancement using one-dimensional photonic crystals. Since one-dimensional photonic crystals will make the excitation electric field intensity will be precisely the same in one plane, ensuring the same fluorescence excitation enhancement multiplier in the same plane. In addition, we design two photonic crystals with high reflectivity to excitation light and high transmittance to emission light versus high transmittance to excitation light and high reflectivity to emission light through the genetic algorithm-assisted design of photonic crystal parameters and combine the two photonic crystals to achieve an upper limit beyond the excitation enhancement of a single common photonic crystal due to the resonant cavity. Compared to some works with a high Q factor [31,32]. It is worth stating that these designs focus on the source in the cavity. The walls of the optical cavity can own the high reflection for the wavelength of the source, however, our design is aiming for two wavelengths whose dipole source is in the cavity, and the plane wave is out of the cavity. These are the two main processes of photoluminescence. Because the plane wave is out of the cavity, we need to ensure the plane wave passes the back-forward photonic crystal first, which needs a low reflection of the back-forward photonic crystal. As a result, we have a lower Q factor than previously observed.

## 2. Materials and Methods

The finite difference time domain method is one of the effective methods to solve the complex electromagnetic environment generated by the interaction of electromagnetic waves with the matter, and in principle, it can solve the problems of arbitrary forms of electromagnetic fields and electromagnetic wave technology. The finite-time difference method takes a discrete approach to the E and H components of the electromagnetic field with alternate sampling in space and time, and in this way, the Maxwell rotational equations with time variables are transformed into a set of difference equations, and the spatial electromagnetic field is solved step by step in the time axis.

The genetic algorithm [33], as a traditional optimization algorithm, is suitable for problems with a moderate number of optimization parameters. The algorithm filters the excellent set of parameters by the fitness function and generates and retains parameters by cross-variance and genetics. The parameters that we optimize by the algorithm are shown in the Table 1. The fitness function reflects the performance of the corresponding parameter structure (The algorithm flow is shown in Supplementary Section S1: Genetic Algorithm).

Here we use the finite difference time domain method to calculate the excitation light reflectance $R_{c1p}$ of the forward photonic crystal; the transmittance $T_{c1d}$ of the forward photonic crystal point source; the extreme value $E_{max}$ of the square of the enhanced electric field mode generated by the combination of the backward photonic crystal and the forward photonic crystal; and the reflectance $R_{c2d}$ of the back photonic crystal point source. The plane wave approximation represents the value of $R_{c2d}$ (the explanation of this method is given in Supplementary Section S2: Plane wave approximation of spherical waves), and the fitness function is defined by the product of the transmission and reflection values of the

corresponding photonic crystal, as shown in Equations (1) and (2). A high $fitness_{c1}$ resulting from the optimization of the genetic algorithm means that the forward photonic crystal has a high reflectance of the excitation light and high transmittance of the emission light, and a high $fitness_{c2}$ means that the backward photonic crystal has high transmittance of the excitation light and high reflectance of the emitted light. Overall, these elements reflect the performance of the structure. The $R_{c1p}$ and $E_{max}$ respond to the properties of the structure excitation process. $R_{c1p}$ is related to forward photonic crystals only; $E_{max}$ is related to forward and back-forward photonic crystals. The $R_{c2d}$ and $T_{c1d}$ respond to the properties of the structure emission process. $R_{c2d}$ is related to back-forward photonic crystals only; $T_{c1d}$ is related to forward photonic crystals only. We calculate different simulation files with a plane wave or dipole, which include one or more parts of the forward PC, backward PC, and layer of the fluorescent solution.

**Table 1.** Parameters for genetic algorithm optimization.

| Parameter | Description |
|---|---|
| $d_{TiO2_f}$ | The thickness of $TiO_2$ for forward photonic crystal |
| $d_{Al2O3_f}$ | The thickness of $Al_2O_3$ for forward photonic crystal |
| $d_{SiO2_f}$ | The thickness of $SiO_2$ for forward photonic crystal |
| defect_f | Forward photonic crystal with defects (Yes or No) |
| $d_{TiO2_b}$ | The thickness of $TiO_2$ for back-forward photonic crystal |
| $d_{Al2O3_b}$ | The thickness of $Al_2O_3$ for back-forward photonic crystal |
| $d_{SiO2_b}$ | The thickness of $SiO_2$ for back-forward photonic crystal |
| defect_b | Back-forward photonic crystal with defects (Yes or No) |

$$fitness_{c1} = R_{c1p} \times T_{c1d} \quad (1)$$

$$fitness_{c2} = E_{max} \times R_{c2d} \quad (2)$$

All materials we selected are based on low prices and are easy to access. The $Al_2O_3$ [34], $SiO_2$ [35], and $TiO_2$ [36] have these characteristics (the index of materials will be shown in the Supplementary Document Section S3: Index of materials in 400–600 nm)

## 3. Results

### *3.1. Photonic Crystal Properties and Performance of the Sandwich Structure*

We assume that the layer of the fluorescent solution was about 3.18 um thick, and the refractive index of Rhodamine 6G was nearly 1.593 at 553 nm and 1.4 at 528 nm [37,38]. After the genetic algorithm-assisted design, we finalized the photonic crystal parameters, as shown in Figure 1a,b, and the transmittance and reflectance of the corresponding two photonic crystals for the excitation wavelength vicinity. It can be found that the backward photonic crystal has a high transmittance near the excitation wavelength of 528 nm, while the forward photonic crystal has a high reflectance.

The overall schematic diagram of the structure is shown in Figure 2a. The excitation light reaches the forward photonic crystal and propagates backward due to the photonic forbidden bands. We indicate the reason for electric enhancement in the layer of the fluorescent solution is the F-P cavity consists of a layer of the fluorescent solution and two photonic crystals. Figure 2d shows that the reflection of the plane wave will cause another change of phase by photonic crystal. The electric field will be enhanced when the phase in the cavity changes by a nearly even number of $\pi$ (detailed proof is available in Supplementary Document Section S4: F-P cavity). The photonic crystals led to a phase difference of 48 degrees, and when the plane wave propagates in the cavity for one cycle, its optical distance was nearly about 33.7 $\pi$. The phase difference caused by the photonic crystal can compensate for the propagating phase difference, which ultimately results in enhanced light field interference. As shown in Figure 2b, the squared value of our electric field mode can reach 10, while it can only reach 4 using a single photonic crystal

(see Supplementary Section S5: Quadruple excitation field enhancement generated by a photonic crystal). Its resonant cavity quality factor Q is about 433.567. Figure 2c, on the other hand, shows the electric field distribution as the exciting electric field passes through the structure in a steady state, reaching the forward photonic crystal with almost zero electric field distribution in front of the forward photonic crystal due to its near 100% reflectivity.

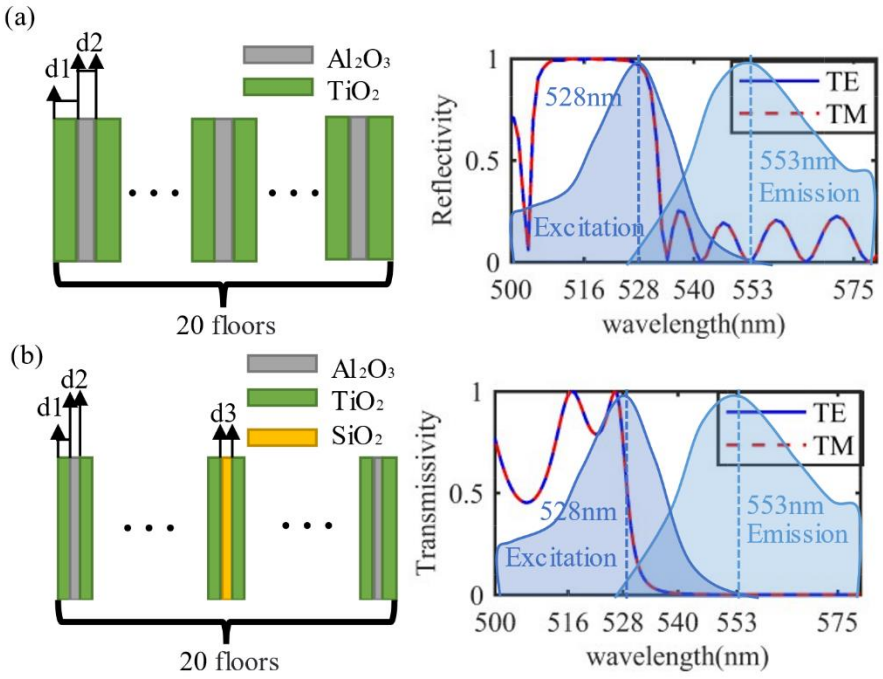



**Figure 1.** Properties of two photonic crystals for exciting light fields. (**a**) Schematic of the forward photonic crystal (d1 = 150 nm; d2 = 108 nm) and its plane wave reflectivity; (**b**) schematic of the backward photonic crystal (d1 = 81 nm; d2 = 61 nm; d3 = 65 nm) and its plane wave transmittance.

Next, we explored the emission process, as shown in Figure 3a; since the electric dipole has three polarization directions, we calculated the distribution of the electric field mode squared under three polarizations at the center of the layer of the fluorescent solution. We can find that our backward photonic crystal has good reflection regardless of the polarization, and this photonic crystal reflects best at small angles. We tested the far-field radiation map of the structure with the same simulation area size, as shown in Figure 3b. We can find that the structure has good directionality and backward photonic crystal reflection under y and z polarization. Still, the backward photonic crystal had poor reflection under x polarization due to the large difference of electric dipole electric field distribution with y and z polarization distribution modes. But all in all, our structure had some light field directionality during emission.

### *3.2. Effect of the Fluorescent Molecule in Different Positions on Fluorescent Light Enhancement Effect*

Since the field strength distribution of the excitation electric field is periodic in the layer of the fluorescent solution, the span of its electric field amplitude of less than 1 is about 35 nm in the weekly period. Here we tested the enhancement effect of the structure on the fluorescent molecule at different positions. We set the structural unit span of 6um at a distance of 12 um from the fluorescent molecule to set up a monitor of 2 um span to contrast the fluorescence enhancement multiples, as shown in Figure 4a,b, we tested the enhancement multiples of the three polarizations at different positions, respectively. The total enhancement multiplier equation of the structure is shown in Equation (3) [39].

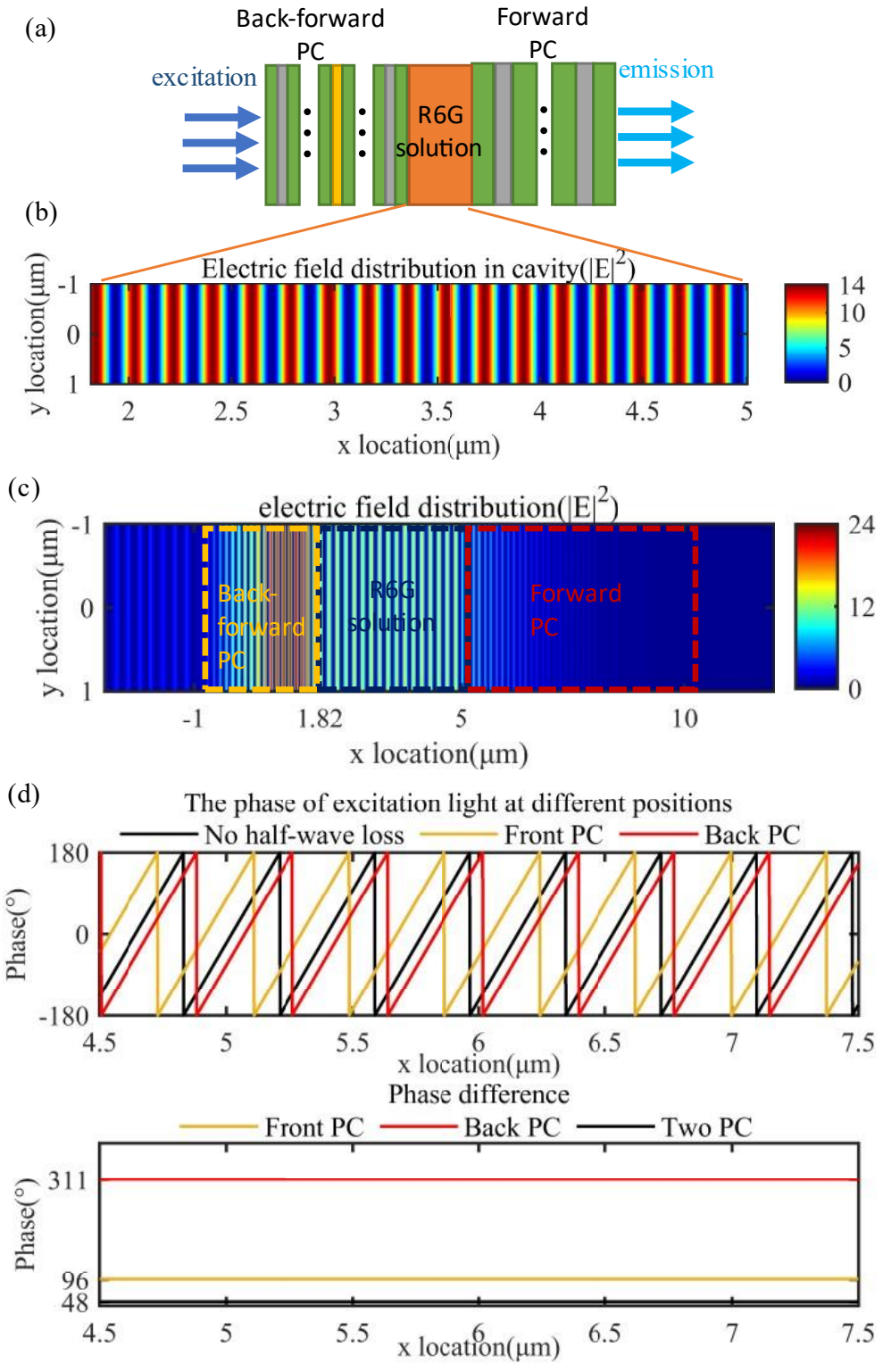



**Figure 2.** Performance of the structure during excitation. (**a**) Schematic diagram of the structure; (**b**) excitation electric field distribution in the layer of the fluorescent solution (partially enlarged); (**c**) overall electric field distribution at the excitation wavelength; (**d**) phase and phase difference after reflection from photonic crystal.

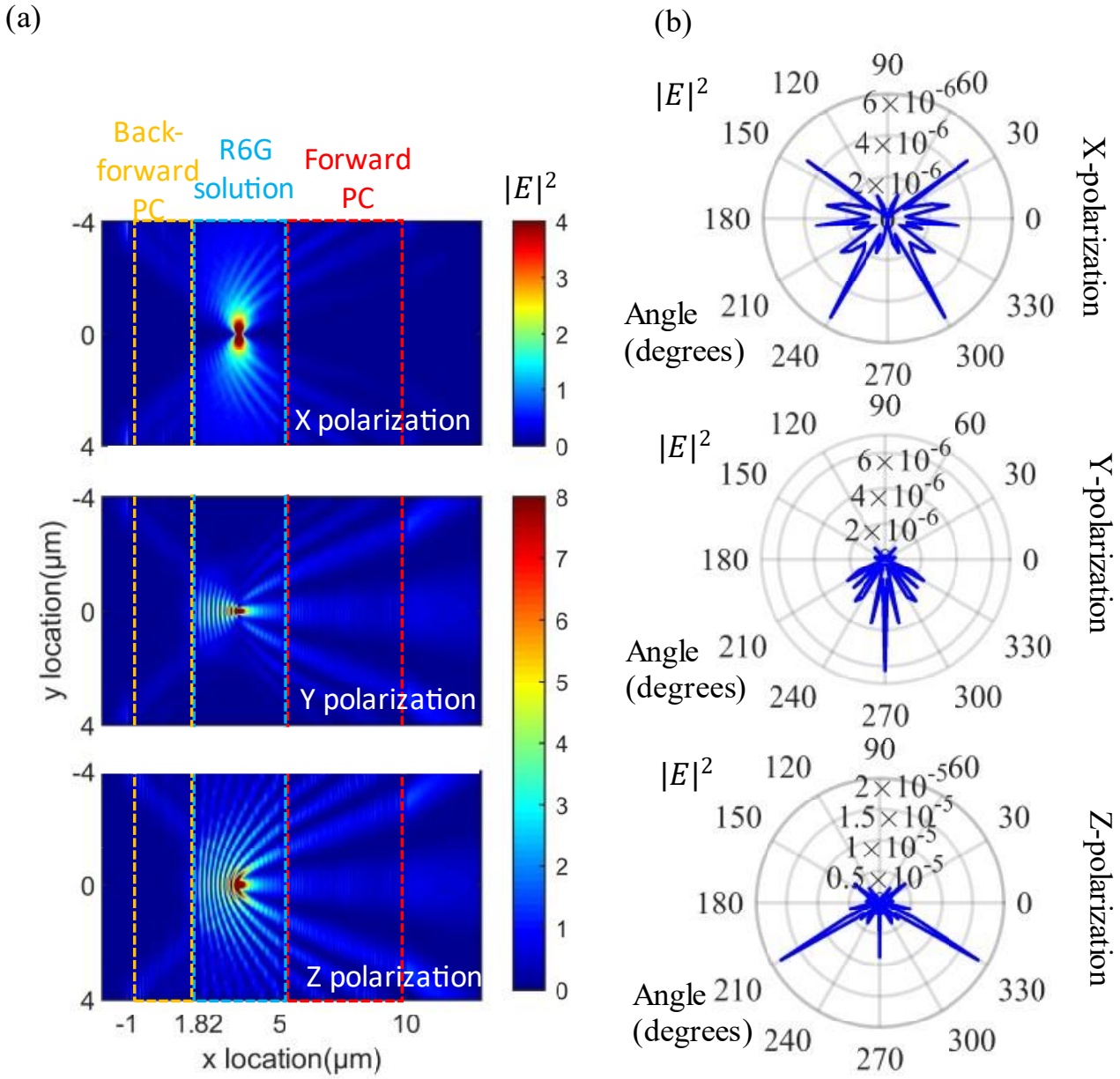



**Figure 3.** Performance of the structure during emission; (**a**) emitted electric field diagram at three polarizations; (**b**) far-field polar coordinates diagram at three polarizations.

$$R_{total} = R_{Excitation} \times R_{Emission} \quad (3)$$

where $R_{Excitation}$ is the enhancement multiplier of the excitation electric field mode squared, and $R_{Emission}$ is the emission electric field enhancement multiplier. Thus, our structure can achieve about 80% of the fluorescent molecules in the enhancement region.

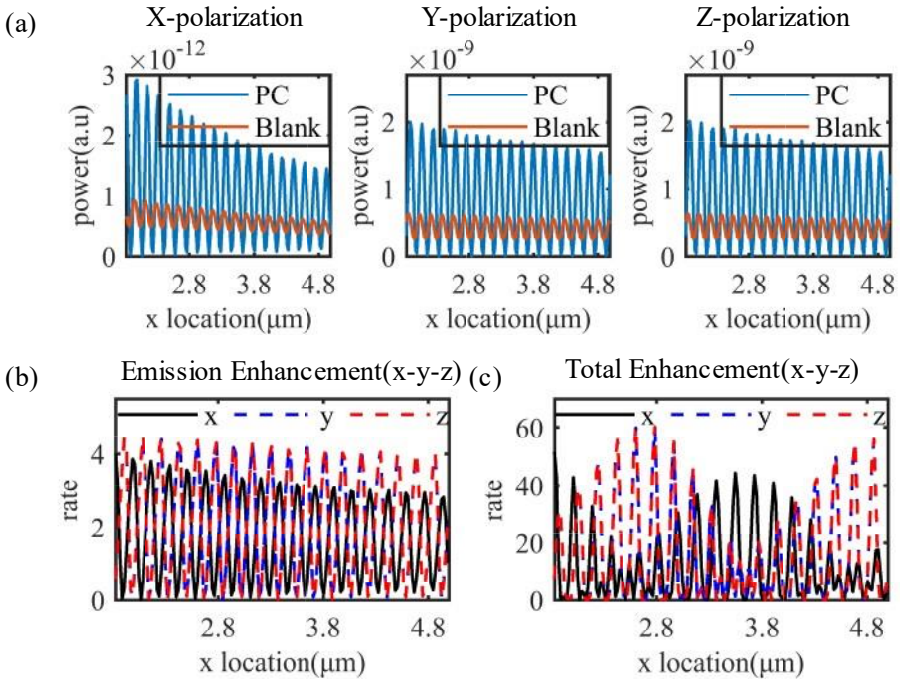



**Figure 4.** Power value and enhancement multiplier at different positions. (**a**) Power value; (**b**) emission enhancement multiplier; (**c**) overall enhancement multiplier.

The final total enhancement multiplier $R_{total}$ versus position is shown in Figure 4c.

Through simulations, we found that the enhancement multiplier of the fluorescent molecule at different positions is not positively correlated with the distance to the backward photonic crystal, but shows a periodic trend (to prove that this phenomenon is not accidental, we verified it in Supplementary Section S6: Effect of reflective structure on the fluorescence enhancement effect at different heights). Here we explain it qualitatively using the Huygens–Fresnel principle, as shown in Figure 5a. Since the distance H of the fluorescent molecule from the backward photonic crystal is constantly changing, the optical field difference between the wave propagating forward to the photonic crystal and the wave propagating forward again after reflection from the backward photonic crystal depends on 2 × H. Therefore, they cancel when the optical range difference corresponds exactly to the phase change$\pi$and increase when the optical range difference is 0. In Figure 4a,b, we can find that the curve changes with a period of about 180 nm, while the half period of the equivalent wavelength of the emitted field among the layer of the fluorescent solution is equal to 173 nm. In addition, the extreme point of the curve under x polarization is different from that under y and z polarization, which is due to the different electric field distribution between x polarization and y and z polarization, as shown in Figure 5b. Therefore, the question of which position will lead to the dominance of phase extinction is somewhat different for x-polarization than for y and z polarization, but the periodicity of their variations is all of half equivalent wavelength. Thus the overall enhancement multiplier for different positions of the structure is shown in Figure 4c, and we achieve the enhancement effect in most of the positions, and the maximum enhancement multiplier can reach 60-fold.

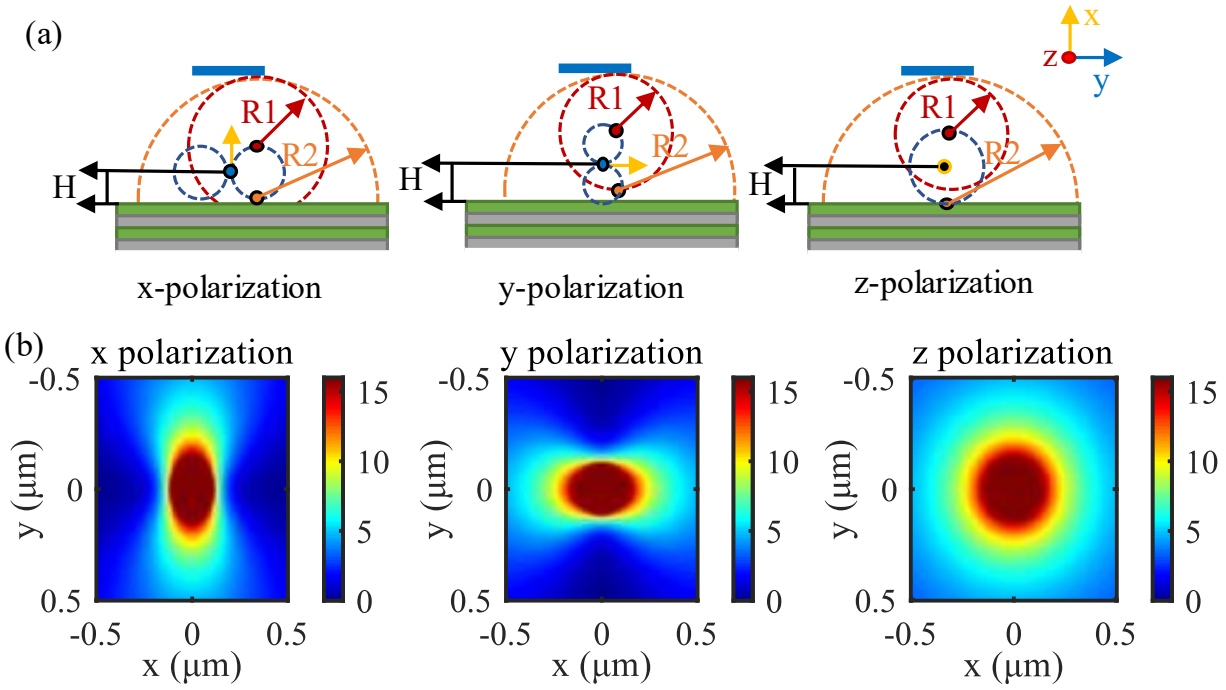



**Figure 5.** Analysis of the enhancement effect at different positions of fluorescent molecules. (**a**) Schematic diagram of the enhancement effect using the Huygens-Fresnel principle under three polarizations; (**b**) electric field intensity distribution under three polarizations.

## 4. Conclusions and Discussion

In summary, we designed a one-dimensional photonic crystal large-volume fluorescence enhancement structure containing a Rhodamine 6G (3.18 μm). By adjusting the photonic crystal parameters and considering the introduction of defects through the genetic algorithm-assisted design, the large-volume enhancement of Rhodamine 6G is finally achieved by combining the optical resonant cavity under the action of the forbidden band and the conduction band of the photonic crystal. Through numerical calculations, we can achieve a maximum of 60-fold enhancement under x, y, and z polarizations. We analyzed the enhancement conditions of the excitation electric field in the FP cavity. We also illustrate the periodic enhancement characteristics of the reflective fluorescence enhancement structure at large volume enhanced fluorescence and perform a qualitative analysis. This design can be used in fields such as displays and further improve device lifetime.

**Supplementary Materials:** The following supporting information can be downloaded at: https://www.mdpi.com/article/10.3390/ma15217803/s1. Ref. [40] was included in Supplemental File.

**Author Contributions:** Conceptualization, G.F. and Z.C.; data curation, J.S., G.F. and Z.C.; formal analysis, J.S.; project administration, J.S.; software, J.S. and H.H.; validation, X.L. and H.H.; visualization, J.S.; writing—original draft, J.S.; writing—review and editing, G.F., X.L. and Z.C. All authors have read and agreed to the published version of the manuscript.

**Funding:** This work was supported by the National Natural Science Foundation of China (62175178, 61971300, 61905208); the Central Guidance on Local Science and Technology Development Fund of Shanxi Province (YDZJSX2021A013); and the Program for the Top Young Talents of Shanxi Province; Program for the Sanjin Outstanding Talents of China.

**Institutional Review Board Statement:** Not applicable.

**Informed Consent Statement:** Not applicable.

**Data Availability Statement:** The data presented in this study are available in Supplementary Materials.

**Conflicts of Interest:** The authors declare no conflict of interest.

## References


1. Wang, M.; Kong, D.; Su, D.; Liu, Y.; Su, X. Ratio fluorescence analysis of T4 polynucleotide kinase activity based on the formation of a graphene quantum dot-copper nanocluster nanohybrid. *Nanoscale* **2019**, *11*, 13903–13908. [CrossRef] [PubMed]
2. Ran, H.; Lin, Z.-Z.; Yao, Q.-H.; Hong, C.-Y.; Huang, Z.-Y. Ratiometric fluorescence probe of MIPs@CdTe QDs for trace malachite green detection in fish. *Anal. Bioanal. Chem.* **2019**, *411*, 537–544. [CrossRef] [PubMed]
3. Wu, W.-L.; Ma, H.-L.; Xi, L.-L.; Huang, M.-F.; Wang, K.-M.; Miao, J.-Y.; Zhao, B.-X. A novel lipid droplets-targeting ratiometric fluorescence probe for hypochlorous acid in living cells. *Talanta* **2019**, *194*, 308–313. [CrossRef] [PubMed]
4. Cui, Y.; Liu, R.; Ye, F.; Zhao, S. Single-excitation, dual-emission biomass quantum dots: Preparation and application for ratiometric fluorescence imaging of coenzyme A in living cells. *Nanoscale* **2019**, *11*, 9270–9275. [CrossRef] [PubMed]
5. Wu, X.; Zeng, L.; Chen, B.-Q.; Zhang, M.; Rodrigues, J.; Sheng, R.; Bao, G.-M. A selective cascade reaction-based probe for colorimetric and ratiometric fluorescence detection of benzoyl peroxide in food and living cells. *J. Mater. Chem. B* **2019**, *7*, 5775–5781. [CrossRef] [PubMed]
6. Hui, K.N.; Fu, W.Y.; Ng, W.N.; Leung, C.H.; Lai, P.T.; Wong, K.K.Y.; Choi, H.W. Polychromatic light-emitting diodes with a fluorescent nanosphere opal coating. *Nanotechnology* **2008**, *19*, 355203. [CrossRef]
7. Aslan, K.; Lakowicz, J.R.; Geddes, C.D. Rapid deposition of triangular silver nanoplates on planar surfaces: Application to metal-enhanced fluorescence. *J. Phys. Chem. B* **2005**, *109*, 6247–6251. [CrossRef]
8. Aslan, K.; Leonenko, Z.; Lakowicz, J.R.; Geddes, C.D. Fast and slow deposition of silver nanorods on planar surfaces: Application to metal-enhanced fluorescence. *J. Phys. Chem. B* **2005**, *109*, 3157–3162. [CrossRef]
9. Bian, Y.; Liu, S.; Zhang, Y.; Liu, Y.; Yang, X.; Lou, S.; Wu, E.; Wu, B.; Zhang, X.; Jin, Q. Distance-Dependent Plasmon-Enhanced Fluorescence of Submonolayer Rhodamine 6G by Gold Nanoparticles. *Nanoscale Res. Lett.* **2021**, *16*, 90. [CrossRef]
10. Adawi, A.M.; Lidzey, D.G. Enhancing the radiative decay rate of fluorescent organic molecules using micropillar microcavities and optical nanocavities. *Mater. Sci. Eng. B-Adv. Funct. Solid-State Mater.* **2008**, *149*, 266–269. [CrossRef]
11. Adawi, A.M.; Murshidy, M.M.; Fry, P.W.; Lidzey, D.G. An Optical Nanocavity Incorporating a Fluorescent Organic Dye Having a High Quality Factor. *Acs Nano* **2010**, *4*, 3039–3044. [CrossRef] [PubMed]
12. Chae, W.S.; Lee, M.J.; Kim, K.; Hyun, J.K.; Jeon, S. Metal-induced fluorescence properties of three-dimensionally ordered macroporous silver inverse opal platforms. *Appl. Phys. Lett.* **2016**, *108*, 071909. [CrossRef]
13. Li, D.; Zhou, D.; Xu, W.; Chen, X.; Pan, G.; Zhou, X.; Ding, N.; Song, H. Plasmonic Photonic Crystals Induced Two-Order Fluorescence Enhancement of Blue Perovskite Nanocrystals and Its Application for High-Performance Flexible Ultraviolet Photodetectors. *Adv. Funct. Mater.* **2018**, *28*, 1804429. [CrossRef]
14. Jin, F.; Xu, L.; Zheng, M.L.; Wang, J.X.; Dong, X.Z.; Zhao, Z.-S.; Song, Y.L.; Duan, X.M. Inhibited/enhanced fluorescence of embedded fluorescent defects by manipulation of spontaneous emission based on photonic stopband. *Rsc Adv.* **2017**, *7*, 19737–19741. [CrossRef]
15. Song, B.; Jiang, Z.; Liu, Z.; Wang, Y.; Liu, F.; Cronin, S.B.; Yang, H.; Meng, D.; Chen, B.; Hu, P.; et al. Probing the Mechanisms of Strong Fluorescence Enhancement in Plasmonic Nanogaps with Sub-nanometer Precision. *Acs Nano* **2020**, *14*, 14769–14778. [CrossRef] [PubMed]
16. Song, J.; Kwon, S.; Kim, E.; Kim, B.; Kim, D.-W.; Lee, S.-Y.; Yee, K.-J. Enhanced photoluminescence of MoS2-Au nanostructures: Nanotriangle and nanohole arrays. *Curr. Appl. Phys.* **2020**, *20*, 703–706. [CrossRef]
17. Ganesh, N.; Zhang, W.; Mathias, P.C.; Chow, E.; Soares, J.A.N.T.; Malyarchuk, V.; Smith, A.D.; Cunningham, B.T. Enhanced fluorescence emission from quantum dots on a photonic crystal surface. *Nat. Nanotechnol.* **2007**, *2*, 515–520. [CrossRef]
18. Hu, S.; Xu, H.; Zhou, B.; Xu, S.; Shen, B.; Dong, B.; Yin, Z.; Xu, S.; Sun, L.; Lv, J.; et al. Double Stopband Bilayer Photonic Crystal Based Upconversion Fluorescence PSA Sensor. *Sens. Actuators B-Chem.* **2021**, *326*, 128816. [CrossRef]
19. Nyman, M.; Shevchenko, A.; Shavrin, I.; Ando, Y.; Lindfors, K.; Kaivola, M. Large-area enhancement of far-field fluorescence intensity using planar nanostructures. *Apl Photonics* **2019**, *4*, 076101. [CrossRef]
20. Zhang, W.; Lei, H. Fluorescence enhancement based on cooperative effects of a photonic nanojet and plasmon resonance. *Nanoscale* **2020**, *12*, 6596–6602. [CrossRef]
21. Xuan, H.; Yao, C.; Hao, X.; Liu, C.; Ren, J.; Zhu, Y.; Xu, C.; Ge, L. Fluorescence enhancement with one-dimensional photonic crystals/nanoscaled ZnO composite thin films. *Colloids Surf. a-Physicochem. Eng. Asp.* **2016**, *497*, 251–256. [CrossRef]
22. Mathias, P.C.; Ganesh, N.; Cunningham, B.T. IEEE, Combined enhanced fluorescence and label-free biomolecular sensing with a two-dimensional photonic crystal. In Proceedings of the 2007 IEEE Leos Annual Meeting Conference Proceedings, Lake Buena Vista, FL, USA, 21–25 October 2007; pp. 71–72.
23. Eftekhari, E.; Li, X.; Kim, T.H.; Gan, Z.; Cole, I.S.; Zhao, D.; Kielpinski, D.; Gu, M.; Li, Q. Anomalous Fluorescence Enhancement from Double Heterostructure 3D Colloidal Photonic Crystals-A Multifunctional Fluorescence-Based Sensor Platform. *Sci. Rep.* **2015**, *5*, 14439. [CrossRef]
24. Wu, Y.; Shen, H.; Ye, S.; Yao, D.; Liu, W.; Zhang, J.; Zhang, K.; Yang, B. Multifunctional Reversible Fluorescent Controller Based on a One-Dimensional Photonic Crystal. *Acs Appl. Mater. Interfaces* **2016**, *8*, 28844–28852. [CrossRef] [PubMed]
25. Soboleva, I.V.; Descrovi, E.; Summonte, C.; Fedyanin, A.A.; Giorgis, F. Fluorescence emission enhanced by surface electromagnetic waves on one-dimensional photonic crystals. *Appl. Phys. Lett.* **2009**, *94*, 231122. [CrossRef]
26. Michelotti, F.; Sepe, E. Anisotropic Fluorescence Emission and Photobleaching at the Surface of One-Dimensional Photonic Crystals Sustaining Bloch Surface Waves. *I. Theory. J. Phys. Chem. C* **2019**, *123*, 21167–21175. [CrossRef]

27. Sepe, E.; Sinibaldi, A.; Danz, N.; Munzert, P.; Michelotti, F. Anisotropic Fluorescence Emission and Photobleaching at the Surface of One-Dimensional Photonic Crystals Sustaining Bloch Surface Waves. II. Experiments. *J. Phys. Chem. C* **2019**, *123*, 21176–21184. [CrossRef]
28. Shobudani, K.; Morifuji, M. IEEE, Enhancement of photoluminescence due to one-dimensional photonic crystal. In Proceedings of the 2013 IEEE International Meeting for Future of Electron Devices, Kansai (Imfedk2013), Suita, Japan, 5–6 June 2013.
29. Min, K.; Choi, Y.-K.; Jeon, H. Model calculations for enhanced fluorescence in photonic crystal phosphor. *Opt. Express* **2012**, *20*, 2452–2459. [CrossRef]
30. Danz, N.; Occhicone, A.; Pflumm, C.; Munzert, P.; Michelotti, F.; Michaelis, D. Spectral analysis of organic LED emitters' orientation in thin layers by resonant emission on dielectric stacks. *Opt. Express* **2021**, *29*, 6608–6619. [CrossRef]
31. Nakamura, T.; Takahashi, Y.; Tanaka, Y.; Asano, T.; Noda, S. Improvement in the quality factors for photonic crystal nanocavities via visualization of the leaky components. *Opt. Express* **2016**, *24*, 9541–9549. [CrossRef]
32. Kassa-Baghdouche, L.; Boumaza, T.; Bouchemat, M. Optical properties of point-defect nanocavity implemented in planar photonic crystal with various low refractive index cladding materials. *Appl. Phys. b-Lasers Opt.* **2015**, *121*, 297–305. [CrossRef]
33. Sampson, J.R. *Adaptation in Natural and Artificial Systems (John H. Holland)*; MIT Press: Cambridge, MA, USA, 1976; Volume 18, pp. 529–530.
34. Gervais, F. Aluminum Oxide ($Al_2O_3$). In *Handbook of Optical Constants of Solids*; Palik, E.D., Ed.; Academic Press: Burlington, MA, USA, 1997; pp. 761–775.
35. Philipp, H.R. Silicon Dioxide ($SiO_2$) (Glass). In *Handbook of Optical Constants of Solids*; Palik, E.D., Ed.; Academic Press: Burlington, MA, USA, 1997; pp. 749–763.
36. DeVore, J.R. Refractive Indices of Rutile and Sphalerite. *J. Opt. Soc. Am.* **1951**, *41*, 416–419. [CrossRef]
37. Lu, Y.; Penzkofer, A. Absorption behaviour of methanolic Rhodamine 6G solutions at high concentration. *Chem. Phys.* **1986**, *107*, 175–184. [CrossRef]
38. Hammond, P. Comparison of experimental and theoretical excited-state spectra for Rhodamine 6G. *IEEE J. Quantum Electron.* **1980**, *16*, 1157–1160. [CrossRef]
39. Das, G.M.; Ringne, A.B.; Dantham, V.R.; Easwaran, R.K.; Laha, R. Numerical investigations on photonic nanojet mediated surface enhanced Raman scattering and fluorescence techniques. *Opt. Express* **2017**, *25*, 19822–19831. [CrossRef]
40. Min, C.; Fuli, Z.; Jianwen, D. OPTICS, 18. pp. 88–133. August 2018.